IEEE Robotics and Automation Letters (RA-L) paper, presented at ICRA 2023, London, UK. Cite as RA-L paper.

Offline Programming Guidance for Swarm Steering of Micro-/Nano Magnetic Particles in a Dynamic Multichannel Vascular Model

Myungjin Park, Tuan-Anh Le and Jungwon Yoon *Member, IEEE*

***Abstract*— Magnetically targeted drug delivery (MTD) systems are used in the treatment of various diseases. However, few studies on the targeting of micro-/nano-sized magnetic particles (MPs) inside multi-bifurcations vessel with fluid flow have appeared. Here, we present a user-interface offline programming guidance (OLPG) scheme that controls MPs within a multi-channel dynamic vascular model. The OLPG scheme can simplify the guidance complexity for MTD and overcome the difficulties in real-time sensing of magnetic nanoparticles (MPs). Calibration between real and virtual environments minimizes OLPG errors due to the aggregation properties of the MPs. A Swarm of Aggregated MPs (SAMPs) can be defined experimentally as the equivalent diameter of a single MP. The joystick position is linearly related to the MP magnetic forces of a real electromagnetic actuator. SAMPs were controlled inside the MTD simulator using the joystick and their control commands can be downloaded to the real controller of the *in vitro* multi-channel vessel model. We performed both simulations and *in vitro* studies in the multi-channel vascular model. A user guided MPs to the desired locations in ~50% of simulations and ~49.5% of in vitro studies, in the absence of visual feedback. Also, a realistic 3D blood vessel model was simulated to evaluate the feasibility of the OLPG scheme. Our system has a potential to guide *in vivo* drug delivery.**

***Index Terms*— Targeted drug delivery, Offline programming, Interactive manipulation, Aggregation model, Swarm control**

I. INTRODUCTION

Micro-/nano-magnetic particles (MPs) have received extensive attention given the technological advances in biomedical applications, such as high-precision targeted drug delivery and micro-/nano-manipulations [1, 2]. Magnetic field therapy has no side-effects and the magnetic field can penetrate deep tissues more safely than in other methods. Thus, targeted drug delivery using magnetic fields is being actively studied [3]. However, some issues remain for implementing precise magnetically targeted drug delivery (MTD). The primary difficulty is the requirement of a real-time, high-resolution imaging device for detecting MPs [4]. Since currently available medical imaging devices [5-7] have limitations related to provision of fast high resolution MP position updates, most studies on guidance of MPs [8-10] focus on handling milliscale micro/nanorobots in a static fluid.

The aggregation of magnetic particles and their swarm control can enhance the targeting and actuation efficiency with better imaging quality with higher concentrations, while it can avoid blood clogging problems when the applied magnetic fields turn off. Therefore, pulsed magnetic field functions [11] have been suggested to guide the swarm of micro-/nano particles to a target region inside a Y-channel model by optimizing magnetic force and frequency inside the dynamic fluid. However, since this open-loop control method requires knowledge of the dynamic characteristics of MPs, vessel geometry and flow rates, it is difficult to extend this scheme to a dynamic fluid vessel with multi-bifurcations. Feedback control guidance scheme [12] for swarm guidance of micro-/nano particles have been suggested for use in dynamic fluid flow conditions inside Y-shaped and multi-bifurcation vessels, but these researches are limited to simulation studies due to the difficulties involved in obtaining real-time positional feedback of the swarm of micro-/nanoparticles in a dynamic vascular environment. Recently, magnetic resonance navigation (MRN) method has been suggested for guidance of an aggregate of magnetic nanoparticles (~1.2mm) in a dynamic fluid vessel with multi-bifurcations [13]. A rotating magnetic field has been utilized to control microswarms (~1mm) inside a Y-shaped vessel with dynamic fluid [14], which could be detected using an ultrasonic imaging device. Also, a combination of acoustic and magnetic fields was suggested for guiding microswarms of robots in a dynamic fluid [15]. Despite recent studies, the generation and guidance of aggregated magnetic particles inside multi-bifurcated vessels with fluid flow is still a big challenge for MTD due to the dispersion characteristics of aggregated magnetic particles and the guidance complexity. Thus, a new guidance scheme for aggregated MPs should be considered to overcome these difficulties.

In contemporary robotics, it is considered useful to employ virtual reality within a control loop [16], because simulation technologies combined with virtual environments afford a wide angle of view (AoV) that allows a user to perform various tests without real hardware (i.e., using real-time sensors). In the field of industrial robotics, off-line programming (OLP) is widely used because it provides precise robot control [17]. OLP allows the robot trajectories for virtual tasks to be created independently using a robot cell; these are then uploaded to the real robot that performs the task. OLP thus shifts the programming burden from the robot operator in the workshop

Manuscript received: November 2, 2021; Revised: December 30, 2021; Accepted: January 26, 2022. This paper was recommended for publication by Editor Xinyu Liu upon evaluation of the Associate Editor and Reviewers' comments. This work was supported by the National Research Foundation (NRF) of Korea (2019M3C1B8090798) and Korea Evaluation Institute of Industrial Technology (KEIT) (No. 20003822).

Myungjin Park and Jungwon Yoon are with the school of Integrated Technology, Gwangju Institute of Science and Technology, Gwangju 61005, South Korea (email: skullmath@gist.ac.kr, jyoon@gist.ac.kr). Tuan-Anh Le is with the School of Integrated Technology, Gwangju Institute of Science and Technology, Gwangju 61005, South Korea and Thuyloi University, 175 Tay Son, Dong Da, Ha Noi, Viet Nam. (e-mail: tuananhle@gm.gist.ac.kr or letuananh@tlu.edu.vn).

Digital Object Identifier (DOI): see top of this page.

to the software engineer in the office. OLP can be used to create complex systems, and is efficient and cost-effective when applied to large-volume production [18]. In the medical field, OLP can be applied for ablation path planning/targeting [16]; virtual ablations are performed after identifying the targets. Each surgical plan is transferred to the real world using a clinical electro-anatomical navigation system, which defines optimal ablation targets via personalized, pre-procedural computational modeling. However, as OLP relies heavily on robot and workspace modeling, precise calibration is required to meet the accuracy requirements.

Magnetically targeted drug delivery (MTD) would benefit from OLP. Through implementing OLP, we can guide micro-/nano particles to a desired location inside the vascular using a magnetic guidance simulator without an imaging device. Furthermore, user can easily generate particles' trajectories because user can intuitively steer micro-/nano particles inside the real-time simulator and get visual feedback from the simulator. Thus, this method can simplify the guidance complexity for MTD and overcome the real-time sensing necessity of the feedback control method. To the best of our knowledge, no previous study has reported the swarm steering of MPs inside a multi-channel dynamic vascular model via OLP in the real world.

In this paper, we developed a novel, user-interfaced offline programming guidance (OLPG) scheme for controlling MPs inside a dynamic vascular model. Here, we implement an OLPG scheme *in vitro* and calibrate the process using magnetic fields, while control commands from the MP guidance simulator [12] can be downloaded to a real vascular model for MPs' swarm guidance without real-time imaging. In Section II, the overall concept is explained. Section III introduces the MTD simulator and calibration scheme for intuitive OLP. Section IV includes simulations of the OLPG scheme performed using commercial software (COMSOL Multiphysics), Section V presents the in vitro experimental results, and Section VI presents the 3D simulation result and discussions for in-vivo application and Section VII provides the conclusions with the planned future work.

II. User-interfaced offline-programming Guidance System

The user-interfaced OLPG system for MPs features an MTD simulator with a joystick, a real-world MP guidance control system, and a calibration scheme to minimize modeling errors between the two systems (Fig. 1). When the user controls MPs in the MTD simulator using the joystick, the interaction point of the control interface must be defined. In MP swarm control [12], it is not possible to set the interaction point by continuously measuring the average MP position inside the vascular model; an imaging device that detects individual MPs is lacking. Thus, we set the interaction point to the center point of a swarm of aggregated MPs (SAMP) based on a calibration algorithm with MP aggregation studies (Fig. 1(a)). First, we determined the relationship between the electromagnetic force and joystick position inside the region of interest (Section III D.1). Second, we obtained the equivalent diameter (d_{eq}) of aggregated MPs via an aggregation study (Section III D.2). Third, we assumed that the aggregated MPs moved as a single particle because their properties and sizes are identical based on

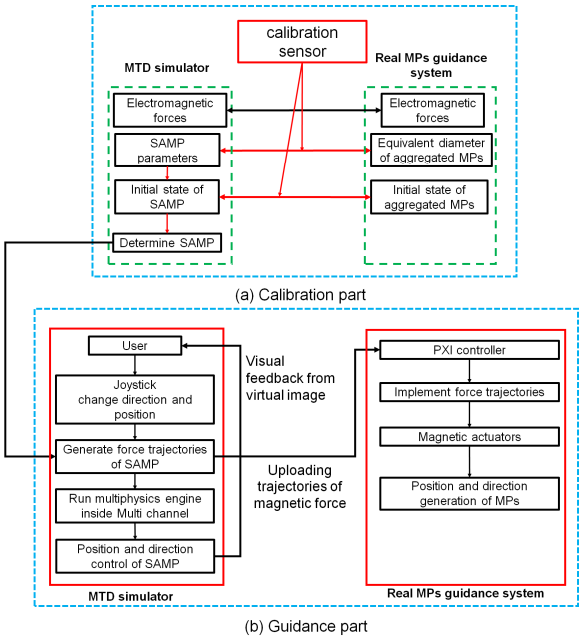

Figure 1. The user-interfaced off-line programming guidance system. (a) Calibration. (b) Guidance.

the d_{eq} of the aggregation model. Thus, the SAMP represents all aggregated MPs inside the vascular model, and is defined as a single particle when the MTD simulator calculates average positions by reference to the d_{eq} of aggregated MPs. When using the SAMP center position as the interaction point, the initial position of that should be obtained via calibration; the position must be identical when all aggregated MPs are injected via an inlet into the *in vitro* system. The user-driven OLPG system is shown in Figure 1(b). Via calibration, we define the SAMP inside the MTD simulator. Then, the user intuitively guides the center SAMP position to the desired location by applying magnetic force to aggregated MPs inside the virtual vascular model. Next, the resultant force trajectories are uploaded to the *in vitro* multichannel guidance control system. Finally, we compare the guidance results of the MTD simulator with those obtained *in vitro* using image processing. Compared to rotating or oscillating magnetic fields [8], the suggested scheme uses a constant magnetic field to generate aggregations of MPs in the calibration stage and uses the gradient field in the guidance stage. Consequently, the aggregated MPs can be steered by changing their radial positions inside the vessel through the gradient magnetic field and the fluid flow can be utilized to propel the aggregated MPs. Whereas, the rotating magnetic field method requires the surface interactions of the substrates of the swarmed MPs for locomotion [8]. Since the proposed guidance scheme does not require the complex locomotion control of MPs inside a vessel with dynamic flow, this can simplify the swarm control of MPs in a dynamic flow compared to the existing swarm controls [9].

III. Intuitive MTD Simulator and Calibration *of in vitro* System

A. Force modeling for steering of MPs in the blood vessel model

Many forces act on MPs moving inside blood vessel model, including hydrodynamic drag and inertial, buoyancy, gravity, adhesion, and contact forces; the hydrodynamic drag,

magnetophoretic, and gravitational forces are the most important. Gravitational force can be the main factor in aggregate formation. Thus, the total force on MPs during particle steering can be derived as:

$$\boldsymbol{F} = \mathbf{F}_{\mathrm{MAP}} + \mathbf{F}_{\mathrm{drag}} + \mathrm{F_m} + \mathrm{F_{etc}} \quad (1)$$

where $\mathrm{F_{MAP}}$ is the magnetophoretic force, $\mathrm{F_m}$ is the gravitational force, and $\mathrm{F_{drag}}$ is the hydrodynamic drag force. $\mathrm{F_{etc}}$ includes the un-modeled forces like dipole force, contact-adhesion force and normal force from the substrate. These forces are neglected due to their small contribution in generation of the overall MPs trajectory, as compared to the magnetic gradient field [21]. In addition, we have assumed elastic boundary conditions for the vascular environment [30]. As the MPs are spherical, lift, the side fluidic forces, and all three fluid moments can be ignored. Each MP is only subjected to the fluid drag force. During MP steering, viscous effects predominate. The drag force on the particles is derived using Stokes' Law as:

$$\mathbf{F}_{\mathrm{drag}} = -3\pi\eta d\left(v_p - v_f\right) \quad (2)$$

where η is the fluid viscosity, d is the MP diameter, v_p is particle velocity, and v_f is the fluid velocity. The gravity and buoyancy forces determine the gravitational force:

$$\mathrm{F_m} = \frac{1}{6}\pi d^3(\rho_p - \rho_s)G \quad (3)$$

where d is the MP diameter, and ρ_p and ρ_s are the MP and fluid densities respectively. The magnetic force $\mathbf{F}_{\mathrm{MAP}}$ is given by:

$$\mathbf{F}_{\mathrm{MAP}} = V(\boldsymbol{M}\cdot\boldsymbol{\nabla})\,\boldsymbol{B} \quad (4)$$

where V is the MP volume, $\boldsymbol{M}$ is the net magnetic polarization, and $\boldsymbol{\nabla}$B is the magnetic gradient field. This simplifies to:

$$\mathbf{F}_{MAP} = \frac{1}{6}\pi d^3 \mu_0 \mathrm{M(H)}\boldsymbol{\nabla H} \quad (5)$$

where μ_0 is the permeability of free space, $\boldsymbol{H}$ is the magnetic intensity, d is the particle diameter, and $\nabla\boldsymbol{H}$ is the magnetic intensity gradient. $\boldsymbol{M(H)}$ is proportional to the magnetic intensity (< 50mT) and we can assume that this is saturated at 60kA/m (> 50mT) [19].

B. Real-time MTD simulator

Our MTD simulator (Fig. 2(a)) [12] features a virtual multi-channel vascular model providing visual information, a simulation engine that accurately reflects MTD dynamics, and a user input device that adjusts magnetic force magnitude and direction. The simulation engine for three-dimensional MP guidance is divided into graphics and physics engine (Fig. 2(b)). The physics engine simulates MPs movements based on fluid dynamics and external magnetic forces. The graphics engine generates visual feedback for the user. The both physics engine and graphics engine were developed using C# programming in Visual Studio 2019 and operates at 1kHz. The position of all MPs are transmitted to the graphics engine. Figure 2(c) shows a flowchart of the physics engine. Before the simulation is run, the user sets parameters for MPs and the vessel (Table I). Then, a fluid velocity profile is generated by COMSOL and this exported to the MTD simulator based on tiny meshes prior to simulation (offline). When simulation commences, the drag force is calculated based on the fluid velocity profile, and the joystick controls the magnitude and direction of the magnetic force (online). Furthermore, the gravitational force is applied based on the parameters listed in Table I.

TABLE I
EXPERIMENTAL PARAMETERS

PARAMETER	Value
MP initial diameter (d_i)	1μm
Water viscosity	0.000894Pa·s
Glycerol + Water (1:1) viscosity	0.004Pa·s
μ_0	$4\pi \times 10^{-7} N/A^2$
Particle density (ρ_p)	2250kg/m^3
Water density (ρ_s)	997kg/m^3
Glycerol + Water density (ρ_s)	1112kg/m^3

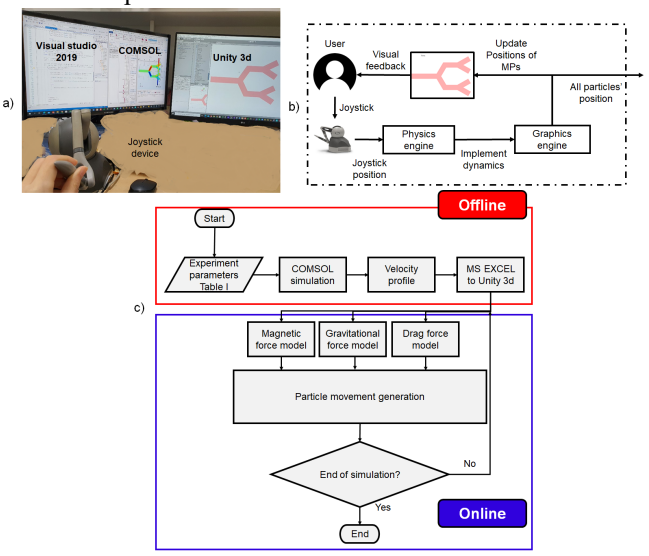

Figure 2. The MTD system. Overall view (a). The simulation engine (b). Flow chart of the physics engine (c).

C. Modeling virtual vascular with flow fluid and in vitro implementation

The COMSOL fluid dynamics of vessel flow can be implemented in a real *in vitro* vessel. We used 3D CAD software (SolidWorks) to design a three-dimensional multichannel vascular model (Fig. 3(a)), and the polydimethylsiloxane (PDMS) chip shown in Fig. 3(b) was manufactured. The remaining lengths have co-length (5mm) and co-diameter (2mm). Figure 3(c) illustrates the computed flow velocity profile inside the channel that shows a low velocity near the walls and a higher velocity in the center of the channel. One inlet was used for continuous water injection, and the other was used for single-step MP injection. We aimed to create identical virtual and real vessels in terms of fluid velocity and geometry.

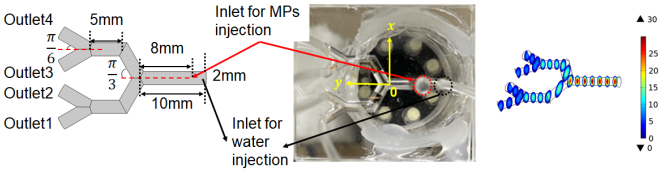

Figure 3. The multichannel geometry; (a) the virtual environment and (b) the real-world environment. (c) The volumetric flow field in the multichannel environment (mm^3/s).

D. Calibration of MP force modeling

For implementing the OLPG scheme for MTD, a precise calibration between the virtual and real vessels is essential.

1) *Electromagnetic force generation using a joystick*

MPs become magnetically saturated during MTD using high fields. As shown in Eq. (5), magnetic force is influenced mainly by the gradient field. We measured the magnetic field (mT) every 5 mm in the regions of interest (ROIs) of the magnetic actuators using a Gauss/Tesla meter (FW BELL 5180) (Fig. 4(a) and (b)). The magnetic field is shown in Figure 4(b). As the coils used not in the precise Maxwell configuration, the gradient field was not constant within the ROIs. The gradient

field depended on MP location and the applied current. That current in the magnetic actuators was determined by joystick

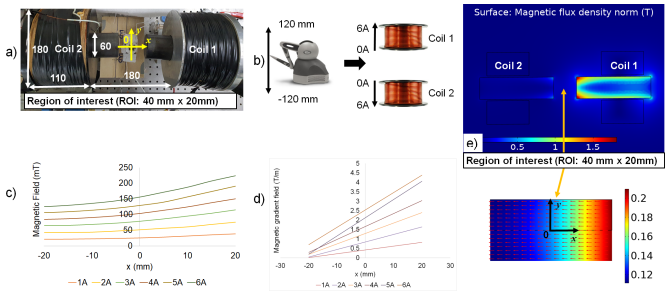

Figure 4. The electromagnetic actuation system. (a) The system for offline programming. (b) Mapping between the workspace of the joystick and the electromagnetic actuation current. The spatial distribution of (c) the magnetic field and (d) the gradient field, when a current of 1–6 A is applied. Magnetic flux distribution for steering of MPs to the right with 6A current applied to coil 1 (e).

position (Fig. 4(c)).

2) *Aggregation of MPs*

Under the external magnetic field, MPs become aggregated via a dipole force [20], and the saturated degree of aggregation depends on the magnetic field, particle size and concentration. In the calibration stage, when the single coil turns on with the maximum current, MPs are aggregated as rod-shaped magnetic chains orientated in the direction of the magnetic field, and the aggregation is saturated as a constant shape after a short period of a few milliseconds. In the guidance stage, the currents in the pair of coils can be changed according to the joystick position. During this stage, we can assume that the equivalent diameter of the aggregated MPs will not change as long as the magnetic field generated by the electromagnetic actuator is lower than the maximum magnetic field applied during the calibration stage (Eq.8). After the end of the guidance stage, MPs become dispersed and disaggregated when the currents of the coils are turned off.

Therefore, we modeled the aggregated MPs as the equivalent diameter (d_{eq}) of a single MP, which can be obtained experimentally [21] (see Fig.5). MPs are aggregated as rod-shaped and each MP of aggregated MPs has an initial diameter d. The equivalent diameter of aggregated MPs is determined by n_2d and the height n_1d. n_1 is the number of MPs in the horizontal direction; n_2 is the number in the vertical direction (Fig. 5). The aggregated MP volume is $\pi/4(n_1n_2^2d^3)$ and the d_{eq} is thus given by:

$$d_{eq}=\sqrt[3]{\frac{3}{2}n_1n_2^2}d \tag{7}$$

We take $\sqrt[3]{\frac{3}{2}n_1n_2^2}$ as the equivalent coefficient (n) for aggregated MPs with a d_{eq} of nd. When considering aggregation effects, the forces acting on aggregated MPs are found by using d_{eq} rather than d in Eqs. (2), (3), and (5). To determine the d_{eq} of aggregated MPs, we performed a simple experiment based on the fluid velocity and particle concentration of the *in vitro* experiment in Section V (Fig. 5(b)). Water continuously injected from inlets with fluid velocity inside the channel (Fig. 3(c)). MPs were injected into the center inlet (Fig. 5(b), white dot circle) and aggregated by applying the maximum magnetic field (6A; 200mT) during 10s (Fig. 5(b2)). After the aggregates of MPs were formed, an opposite magnetic force was applied to move the magnetic particles towards the opposite wall (Fig. 5(b3)). Each aggregate of MPs has a different d_{eq}. To get the

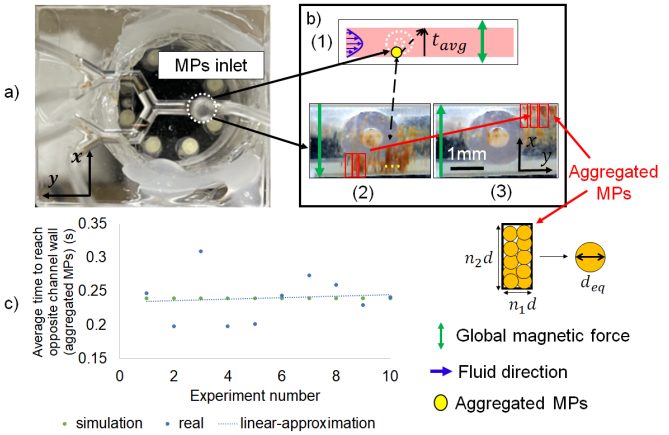

Figure 5. Average time taken by aggregated MPs to reach the opposite wall (t_{avg}) in the MDT simulator (s) and in the *in vitro* environment under an external magnetic field with dynamic fluid conditions. The equivalent diameter (d_{eq}) was 19μm, based on both the simulation and experimental results. (a) The real channel. (b) The aggregation study protocol (enlarged image near the MPs inlet). (c) Reaching time comparison between the simulation and the real-world experiment.

average d_{eq} of aggregated MPs, the average time to reach the opposite wall was estimated and denoted as t_{avg} (Fig. 5(c)). The average d_{eq} was 19μm and t_{avg} was 0.25s, which were obtained through both the simulations and the *in vitro* experiments (Fig. 5(c)). We repeated the procedure ten times to determine the average equivalent diameter (Fig. 5(c)).

The aggregation between magnetic particles is related with magnetic coupling parameter Γ [22]:

$$\Gamma=\frac{\mu_0 \mathrm{M(H)}^2}{2\pi d^3 k_B T} \tag{8}$$

where k_B is the Boltzmann constant, T is temperature, M(H) is the magnetization of MP, and μ_0 is the magnetic permeability of free space. Physically, $\Gamma \gg 1$ corresponds to a situation dominated by magnetic interactions, whereas at $\Gamma \ll 1$, thermal agitation becomes dominant only when magnetization approaches zero. After the aggregated MPs reach the equilibrium state at the maximum magnetic field (200mT), the aggregates will be formed. Then, if the minimum magnetic field is higher than 30mT and the magnetic coupling parameter (Γ) satisfies the condition ($\Gamma \gg 1$), the aggregation of MPs will maintain a constant size. It should be noted that the magnetic field during the guidance stage needs to be between 30mT and 200mT.

E. Calibration of the SAMP center position

Using the experimentally determined d_{eq}, we represented the aggregated MPs as a SAMP that moved like a single particle (Fig. 6(a)). Although the SAMP can represent aggregated MPs inside a vessel, portion of MPs are not aggregated and thus, the SAMP of the MTD simulator does not represent non-aggregated MPs inside a vessel. Furthermore, it is impossible to control both non-aggregated and aggregated MPs with different d_{eq} using a global magnetic field. Consequently, SAMP can only represent aggregated MPs. The SAMP was assumed to be a single particle with the average d_{eq} of aggregated MPs under a magnetic force inside the vessel (Fig. 6(a)). Additionally, initial SAMP position should be determined in calibration stage. Specifically, first, water was continuously injected with target velocity through one inlet. Then, MPs were injected into another inlet (see Fig. 3) and the magnetic field is kept in the negative y-direction to hold the MPs at the channel wall (Fig. 6(b)). Finally, we estimated the initial average

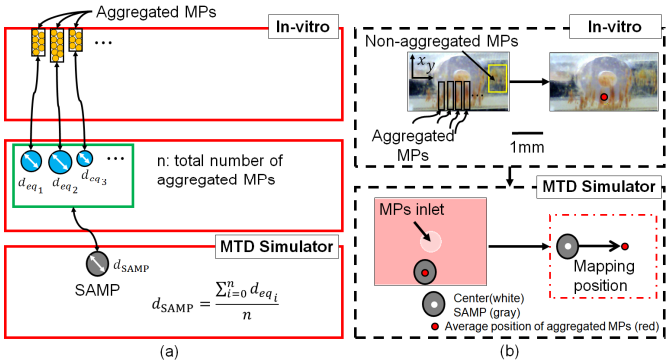

Figure 6. SAMP calibration. (a) Definition of the SAMP and (b) setting of the initial SAMP position.

position of the aggregated MPs using a microscope (SMTUSCOPE; Shenzhen Qi Yao Technology Co.,Ltd) installed near the MP inlet and mapping the SAMP center to the average position of the aggregated MPs.

IV. OLP VERIFICATION VIA SIMULATION OF A MULTICHANNEL VASCULAR MODEL

To evaluate the proposed guidance scheme, we compared the SAMP trajectories of the MTD simulator and MP trajectories simulated by COMSOL under the same magnetic fields. Thus, COMSOL simulations served as the testbed for verification of our OLPG scheme. First, using the MTD simulator in Section III-A, the user viewed the visual screen and guided the SAMP to the desired location. During this process, the SAMP is controlled by drag, magnetic, and gravitational forces. The magnetic force is under the user control. At the end of the guidance process, the magnetic force which is generated by the joystick control at guidance process were uploaded to COMSOL. The COMSOL simulations included 500 non-aggregated and 500 aggregated MPs [20]. We defined the non-aggregated MPs with a lower degree of aggregation (1-3μm) than the average equivalent diameter (19μm). Moreover, based on the aggregation study (Fig.5), we assumed that all aggregated MPs exhibit a randomly distributed d_{eq} between 14μm and 24μm. The conditions for both MTD simulator and COMSOL simulation are shown in Tables I and II, and the fluid flow (Fig.3(c)) reflected blood velocity (0.2–10mm/s) [23]. Figure 7 (a) shows the magnetic forces used to steer the SAMP to the desired location in the MTD simulator.

Additionally, we compared the trajectories of SAMP in the MTD simulator and of MPs positions in the COMSOL simulation (Fig.7 (b)). During 10s, constant magnetic field is applied to generate MPs aggregation and to attach MPs to channel wall for keeping initial position of MPs. Although, both the non-aggregated (blue) and aggregated MPs (red) were near the channel wall, non-aggregated MPs are dispersed, move beyond first bifurcation and thus exist near the channel wall toward to outlet4. On the other hand, aggregated MPs are attached instantly to channel wall before reaching to the first bifurcation. The initial SAMP position was defined using the calibration procedure described in Section III E. At 10s, neither

TABLE II
PARAMETERS USED IN THE SIMULATION

PARAMETER	COMSOL	MTD simulator
Aggregated MP diameter	14-24μm	SAMP: 19μm
Non-aggregated MP diameter	1-3μm	

the aggregated nor non-aggregated MPs moved because the flow velocities converged to zero near the channel wall. At t=13.1s, the both aggregated MPs and non-aggregated MPs became dispersed. Aggregated MPs with a similar d_{eq} of 19μm exhibited small trajectory errors compared to the simulated SAMP trajectories. Meanwhile, non-aggregated MPs were not affected by the applied magnetic fields and thus remained near the channel wall. Even though non-aggregated were affected by the applied magnetic fields, they cannot follow desired trajectories of SAMP due to they already passed through first bifurcation during 10s. At t=17.1s, the SAMP and aggregated MPs were located at the same target. The trajectory errors mainly reflect dispersion of aggregated MPs during the

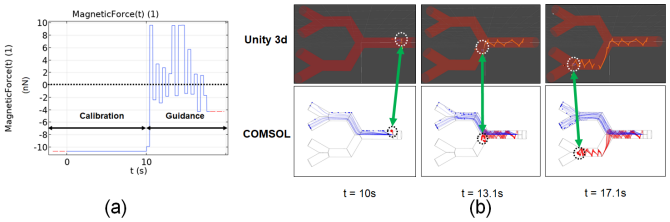

Figure 7. Magnetic force trajectories controlled by the user. (a) MP trajectories of the MTD simulator and COMSOL. (b) The SAMP trajectories (Unity 3d, orange curve), the COMSOL aggregated (red curve) and non-aggregated (blue curve) MPs trajectories. The aggregated and non-aggregated MPs are shown as red and blue spheres, respectively.

COMSOL simulation.

As mentioned in sub-Section III-D, intensity of the magnetic force applied during MTD should be greater than 0.2nN (external magnetic field ~30mT) to maintain MP aggregation. Therefore, the SAMP is always in motion, but its velocity converges to zero at the channel wall. Thus, if the SAMP is close to the channel wall, the user must generate an opposite magnetic force to move it. This explains why the SAMP trajectory zigzags in Figure 7(b).

Table III shows the number of MPs reaching the target at the end of simulation (18s). Non-aggregated MPs ("MPs" in Table III) reached undesired outlets because, as explained above, non-aggregated MPs were not affected enough by the applied magnetic forces and thus had different trajectories than the SAMP. A total of 500 aggregated MPs of 500 MPs ("a-MPs" in Table III) were steered to the desired locations. Although aggregated MPs may become dispersed, because of their small difference of d_{eq}, the SAMP was guided in this manner and thus guided to target location. The COMSOL results showed that most aggregated MPs could be steered via SAMP guidance by exploiting the intuitive trajectory changes of the MTD simulator; non-aggregated MPs were not guided.

TABLE III
VARIATIONS IN MP DISTRIBUTION AT THE END OF THE SIMULATIONS

Fluid	*Particles*	Attaining targets				
		1	**2**	**3**	**4**	**Remain**
Water	na-MPs	0	**0**	314	171	15
	a-MPs	0	**500**	0	0	0

V. IN VITRO RESULTS

A. Experimental setup

External magnetic forces are used to steer MPs in real *in vitro* environments. The electromagnetic actuator has two sets of coils (each with 9300 turns and a diameter of 60mm) with cores (Fig.4(a)) accepting a current of up to 6 A (Fig. 4(b)). Fig.4(c) shows the mapping between the joystick workspace

and coil current intensity. The negative sign indicates a directional change in the magnetic force. A PXI controller and two independent power supplies (Aetechron-7224) were used to control each coil through a LabVIEW interface (Fig.8). MPs 1μm in diameter at 50mg/mL (SIMAG-Silanol 1101; Chemicell, saturation magnetization value: 60kA/m with superparamagnetic hysteresis loop [19]) were injected through a syringe needle (0.02mL). Simultaneously, water was continuously injected via a syringe pump at 0.942 ml/min, identical to the conditions described in Section III and IV. The multichannel was also identical to that of the simulation (Figs.7(b) and 8).

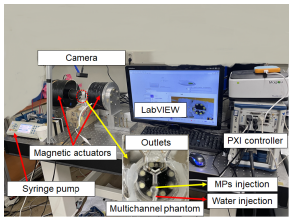

Figure 8. The *in-vitro* system.

To evaluate OLPG efficiency and functionality, we used two test modes. In the Default mode (D), MPs moved without the magnetic guidance. In the OLPG mode, the user steered the SAMP via visual feedback from the virtual screen, and the data were uploaded to the *in vitro* model.

B. Results

We evaluated OPLG performance; the targeting ratio was estimated with ImageJ software (NIH). MPs were injected through an inlet under the maximum constant magnetic field (~200mT) (Fig. 4), which prohibits MPs from flowing with the water and triggers MP aggregation prior to any user command. The initial SAMP position was the same as in the calibration procedure described in Section III-E. Then, the user commands (Fig.7(a)) were uploaded to the PXI controller (Fig.8). The targeting ratio was estimated by measuring the area occupied by MPs, as revealed by an image processing technique using color segmentation (Fig. 9, measuring the pixel areas).

The representative guidance results are shown in Figure 9. In the simulator trial, the SAMP trajectory was divided into 19 representative points. The images show where the MPs are located at each representative point during the *in vitro* experiment. The first point (1) is at the end of the calibration stage (~10s) where a constant magnetic field had been applied and MPs had moved in the upward direction. Point 7 shows that some aggregated MPs became dispersed because of their different d_{eq} and the non-aggregated MPs had already dispersed towards the undesired outlets. The remaining aggregated MPs moved to the desired position following trajectories similar to those in the simulation (point 15). At the final point (19), most of the aggregated MPs existed near the reference point, while the non-aggregated MPs remained at the undesired locations.

Without magnetic field in Default mode, the areas of the four targets occupied by MPs were similar, at 26.2%, 26.9%, 23%, and 23.9% for targets 1–4, respectively (Table IV). The results are similar with simulation results. The OLPG results are shown in Figure 9; about 49.5% of all MPs reached the desired target. After point 15, the MP concentration changed because of the continuous water injection; image processing did not clearly reveal areas covered by MPs. Therefore, we calculated the results at point 15. We first measured the area (941 pixels) occupied by MPs at the calibration stage (point 1). Unlike in the COMSOL simulation, MPs did not remain close to the channel wall because they were under an injection force, and had already dispersed toward target 4. After guidance to point 15, the area occupied by MPs near the desired target 2 was 466 pixels; (466 × 100/941 = 49.5%). The value for target 4 was 421 pixels (44.7%). The remaining area was 54 pixels (941 – 466 - 421 = 54).

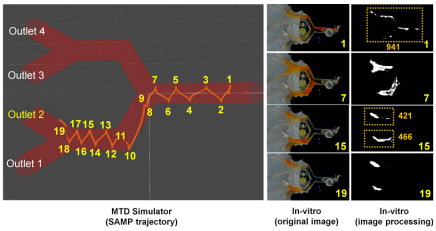

Figure 9. OLPG implementation *in vitro*. Simulated SAMP trajectories, MP images obtained *in vitro* without and with image processing. Outlet 2 was the desired target during both simulation and *in vitro*.

During MTD, this remaining area of MPs passed through the targets and were thus lost. The targeting ratios are shown in Table IV. As for the simulation results (Table IV), the targeting ratios of non-aggregated and aggregated MPs cannot be distinguished *in vitro* due to the uncontrollable characteristics of the non-aggregated MPs and we thus compared the summed targeting ratios. The proportion of MPs reaching the desired target 2 was 50% in the simulation and 49.5% *in vitro*; the respective proportions that reached undesired outlets or remained inside the channel were 50% and 50.5%.

In simulation, the percentage of MPs entering outlet3 and outlet4 can be measured, respectively, but in *in-vitro*, the percentage is estimated through the image processing at the end of calibration stage (10s) and the image after guidance (18s). It is difficult to measure targeting ratio of outlet3 or outlet4 during guidance. Therefore, we compare the sum of outlet3, outlet4 and remaining. It is 50% and 50.5%, which is similar to the simulation result. In other words, the targeting ratio was also 50% and 49.5%, and similar results could be achieved *in-vitro* with simulation result.

To evaluate feasibility of the proposed guidance scheme for *in-vivo* applications, we performed an additional experiment in a solution with blood-like viscosity (glycerol 50% + water 50%, viscosity ~0.004Pa·s), that involved generating the SAMP trajectory (Fig. 10(a)) and uploading the force trajectory (Fig.10 (b)). As compared to water, the 50% glycerol solution requires higher magnetic forces to overcome the drag forces ($F_{rms} = \sqrt{\frac{1}{T_2-T_1}\int_{T_1}^{T_2}[F(t)^2]dt}$, F_{rms} in water: 5.44nN (Fig.7(a)) and F_{rms} in 50% glycerol: 8.88nN (Fig.10(b))). Specifically, during the calibration stage where the maximum magnetic field is applied (point1), the aggregated MPs (red spheres) in 50% glycerol were more dispersed due to the vessel flow (see Fig. 7(a) at t=10s and Fig.10(c) at point 1). In addition, the non-aggregated MPs (blue spheres) in the 50% glycerol were less affected by the magnetic forces. Thus, they were dispersed throughout all the channels, which could be observed in both the simulation (Fig. 10(c)) and the in-*vitro* (Fig.10(d)) results. Due to the initial dispersion at the calibration stage, some aggregated MPs cannot follow the reference trajectory (point 3). Thus, the guidance efficiency in the 50% glycerol is slightly less than that in water. At the end of the guidance stage (point 9), we measured the

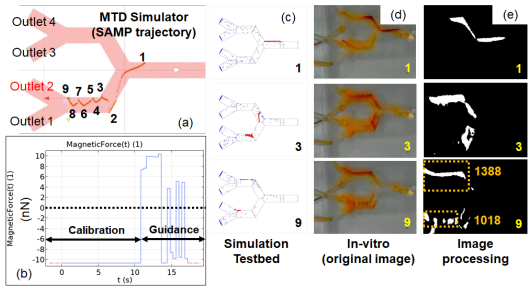

Figure 10. *In vitro* OLPG implementation (blood-like solution). (a) SAMP trajectory. (b) applied magnetic force. (c) COMSOL simulation testbed. (d) *in vitro* image and (e) image processing to determine targeting ratio.

TABLE IV. TARGETING RESULTS DURING IN VITRO AND SIMULATION

Fluid	*Study*	*Mode*	Attainment of target (%)			
			1	2	3	4 or more
Water	Simul	Default	25.2	24.7	26	24.1
		OLPG	0	50	31.4	18.6
	In vitro	Default	26.2	26.9	23	23.9
		OLPG	0	49.5	50.5	
50% glycerol	Simul	Default	25.2	24.7	26	24.1
		OLPG	16.4	46.7	9.2	27.7
	In vitro	Default	24.8	25.1	25.4	24.7
		OLPG	0	42.3	57.7	

pixel area of MPs that had moved towards outlet 2 (Table IV). The results showed that we were able to guide ~ 46% of the MPs to the desired outlet in the simulator and ~42% (1018/2406) in the *in-vitro* experiment. Thus, the proposed guidance scheme is feasible for use in an environment with blood-like viscosity.

VI. OLP STEERING SIMULATION IN A 3D BLOOD VESSEL MODEL AND DISCUSSIONS

A. Simulation in a 3D blood vessel model

To evaluate the feasibility of the proposed scheme in *in-vivo* applications, a simulation was designed in a 3-D realistic channel. The 3-D vessel geometry of a specific vessel of the human brain was selected and extracted using MRI [24]. our guidance approach will be more beneficial to the brain, which is difficult to be accessed through a catheter.

The final 3-D model of the channel is shown in Fig. 11(b) and the velocity inside the channel, computed using the CFD module of COMSOL, is shown in Fig. 11(a). The channel was filled with an environment that has characteristics similar to that of blood (the density was 1050kg/m^3 and the viscosity was 0.004Pa·s). Additionally, we use the six magnetic actuators with cores to consider the 3D steering of MPs [25]. Each coil pair has the same configuration as the current system, as shown in Fig.4. In this simulation, the overall approach is the same as the current system. Moreover, we assumed that current of each set is mapped with the position of the joystick. First, 1000 MPs are injected into the inlet and the maximum constant magnetic force is applied over 0.8s to generate the aggregation of MPs (calibration stage). Second, the force trajectory of SAMP is uploaded to COMSOL (guidance stage). In the simulations, the same particle conditions as Table II were used. Representative results (desired outlet5) were captured after the calibration stage (Fig.11(c)) and the guidance stage (Fig.11(d)), respectively.

The distribution numbers of MPs in all the cases are presented in Table V. Compared to the default mode (no magnetic field), the targeting ratio with the OLPG can be improved by 162 ~ 611%. The number of bifurcations affects the targeting efficiency. From the simulation results of the realistic blood vessel model, we found that the outlets (2,3,4) with two bifurcations have similar targeting efficiencies of 29.6 ~ 65.1%, given in table V, as compared to the 50% (see table IV) observed in the in-vitro experiment with two bifurcations. Whereas, outlet 6 with three bifurcations has only 5% targeting result even though the targeting improvement ratio is above 600%. Modifying the viscosity of the fluid only rescales the equilibrium time of the aggregation process, without modifying the underlying physical mechanism [26]. Thus, high viscosity will require enough magnetic guidance force to overcome the drag force for real in-vivo applications.

B. Discussions for in vivo applications

To extend OLPG in an in-vivo experiment, precise calibration procedures between the simulator and real-environments is inevitable. There are four major calibrations required to apply OLPG in MTD. The first step is to bring the in-vivo model equally into the simulation. Recently, a MRI imaging technique combined with deep-learning is suggested to reconstruct image of brain or complex vessels [24]. Thus, we can reconstruct as virtual image that is the same with real image. The second step is the aggregation modeling. In this paper, we estimate the equivalent diameter through experiment results. However, during MTD, the equivalent diameter may change due to the fluid dynamics effects or geometrical structures. Currently, researchers can estimate the changes of aggregation in a fluid under magnetic field [27]. Thus, by implementing the aggregation model into a MTD simulator, we can get the equivalent diameter precisely. As increasing magnetic field, we can increase portions of the aggregated MPs inside the vascular and higher equivalent diameters of MPs. However, this can cause clogging inside the vascular [28]. The aggregation size should be carefully determined between the guidance efficiency and the safety of patients. It should also be noted that since the particle diameter used for OLPG is 1μm, biocompatible

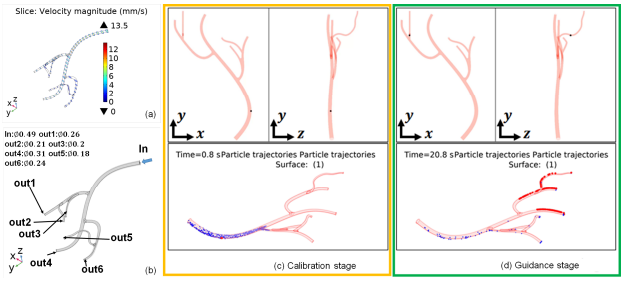

Figure 11. (a) fluid velocity profile. (b) 3-D model of a real vessel from human brain. One representative result both calibration stage (c) and guidance stage (d) (desired location: outlet 5). Black sphere in MTD simulator: SAMP, blue sphere (non-aggregated MPs) and red sphere (aggregated MPs).

TABLE V. PARTICLE DISTRIBUTION

Target	Reaching to outlets						Remained in channel
	1	2	3	4	5	6	
Default	284	53	105	401	9	143	5
1	732	26	40	158	2	25	17
2	299	445	47	153	6	36	14
3	205	36	296	158	6	190	109
4	163	36	51	651	7	36	56
5	184	36	48	203	55	83	238
6	202	36	48	156	6	536	16

nanoparticles with a smaller size (under 200nm) should be considered for in-*vivo* applications [29].

In the third step, precise initial position acquisition of SAMP is also required for precise guidance. Estimated SAMP can be calibrated frequently by the average position of MPs through imaging device. Finally, modeling of the forces acting on nanoparticles should be improved to better simulate the real environment. In this paper, we have considered only the major forces, i.e. gravitational, drag and magnetic forces. However, in real applications, there will be blood pulse and friction [30] with the vascular wall, which also severe to influence the nanoparticles' motion. The wall effect will also have an effect on the drag forces and the friction gradient, which is proportional to the distance between the magnetic particle and the wall [31]. These issues can be solved through consideration of these factors in the simulator or through frequent calibration of the imaging device. Additionally, when we extend the OLPG to a 3D environment, it is essential to extend the actuation system to 3D. A virtual field free point (FFP) for linear control of MPs can be used as a 3D intuitive actuation system [32].

VII. Conclusions and Future Work

We successfully developed a user-interfaced OLPG scheme for swarm guidance of aggregated MPs in multi-bifurcation vessel with flow fluid. Simulation and *in vitro* studies were performed. Precise calibration between the simulator and real vessel is required. MP aggregation study revealed the d_{eq} of MP aggregations and SAMPs. Initial SAMP position was obtained via positional matching of aggregated MPs in the real vascular model. During simulation, the user guided ~50% of all MPs to the target; the *in vitro* value was ~49.5%. The simulation and experimental results were in acceptable agreement. Furthermore, we simulated a 3D realistic vessel model with different dynamic conditions and showed the effectiveness of the OLPG. In future, we will perform in-vitro experiments with more complex vascular models for *in vivo* applications.

References

[1] R. Singh and J. W. Lillard Jr, "Nanoparticle-based targeted drug delivery," *Experimental and molecular pathology,* vol. 86, no. 3, pp. 215-223, 2009.

[2] O. Veiseh, J. W. Gunn, and M. Zhang, "Design and fabrication of magnetic nanoparticles for targeted drug delivery and imaging," *Advanced drug delivery reviews,* vol. 62, no. 3, pp. 284-304, 2010.

[3] Y.-L. Liu, D. Chen, P. Shang, and D.-C. Yin, "A review of magnet systems for targeted drug delivery," *Journal of Controlled Release,* vol. 302, pp. 90-104, 2019.

[4] Q. Wang and L. Zhang, "External Power-Driven Microrobotic Swarm: From Fundamental Understanding to Imaging-Guided Delivery," *ACS nano,* vol. 15, no. 1, pp. 149-174, 2021.

[5] C. Degen, M. Poggio, H. Mamin, C. Rettner, and D. Rugar, "Nanoscale magnetic resonance imaging," *Proceedings of the National Academy of Sciences,* vol. 106, no. 5, pp. 1313-1317, 2009.

[6] T. Saranteas, "Limitations in ultrasound imaging techniques in anesthesia: obesity and muscle atrophy?," *Anesthesia & Analgesia,* vol. 109, no. 3, pp. 993-994, 2009.

[7] T. Sera, "Computed tomography," in *Transparency in Biology*: Springer, 2021, pp. 167-187.

[8] H. Xie *et al.*, "Reconfigurable magnetic microrobot swarm: Multimode transformation, locomotion, and manipulation," *Science Robotics,* vol. 4, no. 28, 2019.

[9] J. Yu, L. Yang, and L. Zhang, "Pattern generation and motion control of a vortex-like paramagnetic nanoparticle swarm," *The International Journal of Robotics Research,* vol. 37, no. 8, pp. 912-930, 2018.

[10] Q. Wang, L. Yang, J. Yu, P. W. Chiu, Y.-P. Zheng, and L. Zhang, "Real-time magnetic navigation of a rotating colloidal microswarm under ultrasound guidance," *IEEE Transactions on Biomedical Engineering,* 2020.

[11] A. K. Hoshiar, T.-A. Le, F. U. Amin, M. O. Kim, and J. Yoon, "A novel magnetic actuation scheme to disaggregate nanoparticles and enhance passage across the blood–brain barrier," *Nanomaterials,* vol. 8, no. 1, p. 3, 2018.

[12] M. Park, T.-A. Le, A. Eizad, and J. Yoon, "A Novel Shared Guidance Scheme for Intelligent Haptic Interaction Based Swarm Control of Magnetic Nanoparticles in Blood Vessels," *IEEE Access,* vol. 8, pp. 106714-106725, 2020.

[13] N. Li *et al.*, "Magnetic resonance navigation for targeted embolization in a two-level bifurcation phantom," *Annals of biomedical engineering,* vol. 47, no. 12, pp. 2402-2415, 2019.

[14] Q. Wang *et al.*, "Ultrasound Doppler-guided real-time navigation of a magnetic microswarm for active endovascular delivery," *Science Advances,* vol. 7, no. 9, p. eabe5914, 2021.

[15] D. Ahmed *et al.*, "Bioinspired acousto-magnetic microswarm robots with upstream motility," *Nature Machine Intelligence,* vol. 3, no. 2, pp. 116-124, 2021.

[16] P. M. Boyle *et al.*, "Computationally guided personalized targeted ablation of persistent atrial fibrillation," *Nature biomedical engineering,* vol. 3, no. 11, pp. 870-879, 2019.

[17] P. Neto and N. Mendes, "Direct off-line robot programming via a common CAD package," *Robotics and Autonomous Systems,* vol. 61, no. 8, pp. 896-910, 2013.

[18] Z. Pan, J. Polden, N. Larkin, S. Van Duin, and J. Norrish, "Recent progress on programming methods for industrial robots," *Robotics and Computer-Integrated Manufacturing,* vol. 28, no. 2, pp. 87-94, 2012.

[19] O. Oduwole, D. T. Grob, and S. Sheard, "Comparison between simulation and experimentally observed interactions between two magnetic beads in a fluidic system," *Journal of Magnetism and Magnetic Materials,* vol. 407, pp. 8-12, 2016.

[20] E. Karvelas, N. Lampropoulos, L. Benos, T. Karakasidis, and I. E. Sarris, "On the magnetic aggregation of Fe3O4 nanoparticles," *Computer Methods and Programs in Biomedicine,* vol. 198, p. 105778, 2021.

[21] A. K. Hoshiar, T.-A. Le, and J. Yoon, "Electromagnetic Actuation Scheme for Swarm of Magnetic Nanoparticles Steering in Multi-bifurcation," in *2019 International Conference on Manipulation, Automation and Robotics at Small Scales (MARSS)*, 2019, pp. 1-6: IEEE.

[22] J. S. Andreu, J. Camacho, and J. Faraudo, "Aggregation of superparamagnetic colloids in magnetic fields: the quest for the equilibrium state," *Soft Matter,* vol. 7, no. 6, pp. 2336-2339, 2011.

[23] W. S. Kamoun *et al.*, "Simultaneous measurement of RBC velocity, flux, hematocrit and shear rate in vascular networks," *Nature methods,* vol. 7, no. 8, pp. 655-660, 2010.

[24] F. Knoll *et al.*, "Deep-learning methods for parallel magnetic resonance imaging reconstruction: A survey of the current approaches, trends, and issues," *IEEE Signal Processing Magazine,* vol. 37, no. 1, pp. 128-140, 2020.

[25] M. D. Tehrani, M. O. Kim, and J. Yoon, "A novel electromagnetic actuation system for magnetic nanoparticle guidance in blood vessels," *IEEE transactions on magnetics,* vol. 50, no. 7, pp. 1-12, 2014.

[26] A. Darras, E. Opsomer, N. Vandewalle, and G. Lumay, "Superparamagnetic colloids in viscous fluids," *Scientific reports,* vol. 7, no. 1, pp. 1-8, 2017.

[27] N. Pei *et al.*, "Aggregation process of paramagnetic particles in fluid in the magnetic field," *Bioelectromagnetics,* vol. 37, no. 5, pp. 323-330, 2016.

[28] Y. Gao, A. van Reenen, M. A. Hulsen, A. M. de Jong, M. W. Prins, and J. M. den Toonder, "Disaggregation of microparticle clusters by induced magnetic dipole–dipole repulsion near a surface," *Lab on a Chip,* vol. 13, no. 7, pp. 1394-1401, 2013.

[29] F. Griese *et al.*, "Simultaneous Magnetic Particle Imaging and Navigation of large superparamagnetic nanoparticles in bifurcation flow experiments," *Journal of Magnetism and Magnetic Materials,* vol. 498, p. 166206, 2020.

[30] E. Boileau *et al.*, "A benchmark study of numerical schemes for one-dimensional arterial blood flow modelling," *International journal for numerical methods in biomedical engineering,* vol. 31, no. 10, p. e02732, 2015.

[31] R. Razaghi and M. H. Saidi, "Experimental investigation of drag and lift forces on microparticles in low Reynolds number poiseuille flow in microchannel," *Journal of Dispersion Science and Technology,* vol. 37, no. 12, pp. 1767-1777, 2016.

[32] M. P. Bui, T.-A. Le, and J. Yoon, "A Magnetic Particle Imaging-based Navigation Platform for Magnetic Nanoparticles using Interactive Manipulation of a Virtual Field Free Point to Ensure Targeted Drug Delivery," *IEEE Transactions on Industrial Electronics,* 2020.